FRONTIERS OF PHYSICS

RESEARCH ARTICLE
Volume 18 / Issue 4 / 42304 / 2023

Quantum multiparameter estimation with multi-mode photon catalysis entangled squeezed state

Huan Zhang[1], Wei Ye[2], Shoukang Chang[3], Ying Xia[1], Liyun Hu[4,†], Zeyang Liao[1,‡]

1 School of Physics, Sun Yat-sen University, Guangzhou 510275, China
2 School of Information Engineering, Nanchang Hangkong University, Nanchang 330063, China
3 MOE Key Laboratory for Nonequilibrium Synthesis and Modulation of Condensed Matter, Shaanxi Province Key Laboratory of Quantum Information and Quantum Optoelectronic Devices, School of Physics, Xi'an Jiaotong University, Xi'an 710049, China
4 Center for Quantum Science and Technology, Jiangxi Normal University, Nanchang 330022, China
Corresponding authors. E-mail: †hlyun@jxnu.edu.cn, ‡liaozy7@mail.sysu.edu.cn
Received October 23, 2022; accepted February 18, 2023

ABSTRACT

We propose a method to generate the multi-mode entangled catalysis squeezed vacuum states (MECSVS) by embedding the cross-Kerr nonlinear medium into the Mach–Zehnder interferometer. This method realizes the exchange of quantum states between different modes based on Fredkin gate. In addition, we study the MECSVS as the probe state of multi-arm optical interferometer to realize multi-phase simultaneous estimation. The results show that the quantum Cramer–Rao bound (QCRB) of phase estimation can be improved by increasing the number of catalytic photons or decreasing the transmissivity of the optical beam splitter using for photon catalysis. In addition, we also show that even if there is photon loss, the QCRB of our photon catalysis scheme is lower than that of the ideal entangled squeezed vacuum states (ESVS), which shows that by performing the photon catalytic operation is more robust against photon loss than that without the catalytic operation. The results here can find applications in quantum metrology for multiparatmeter estimation.

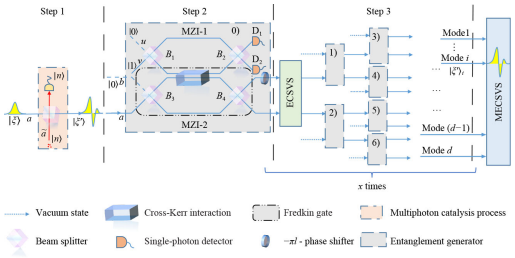

Keywords quantum metrology, squeezing vacuum, quantum catalysis, multi-parameter estimation

1 Introduction

Quantum metrology is one of the most important research fields in quantum information science which can provide significant quantum advantages over its classical counterpart. A fundamental task in quantum metrology is to improve the estimation precision of parameters to be measured through quantum resources allowing by the basic principles of quantum mechanics. Generally speaking, the typical quantum metrology includes three steps: the preparation of probe states, the evolution of probe states, and the readout of the evolved states. In quantum metrology, the quantum Cramer–Rao bound (QCRB) is usually used to quantify the estimation precision offered by quantum metrology, which gives the lower limit of the estimation precision that can be achieved using any possible detection methods [1–5]. For this purpose, prior works are focused on the estimation of a single parameter with superior quantum resources [6–20]. For instance, by adopting nonclassical or entangled states, such as single (two)-mode squeezed vacuum state (S(T)SVS) [11–13] and NOON state [14],

Higher Education Press

arXiv: 2210.15381
https://doi.org/10.1007/s11467-023-1274-6

the estimation precision can overcome the so-called standard quantum limit (SQL) scaling as $1/\sqrt{N}$ with N being the mean photon number of the probe state, and in certain cases, the precision can even approach to the renowned Heisenberg limit (HL) with a scaling $1/N$. If we can perform certain non-Gaussian operations such as photon addition, subtraction and catalysis on the squeezing states, we may further enhance the precision of the metrology [15–20].

In the realistic scenarios, such as biological system measurement [21–23], the optical imaging and the sensor network [24–28], multiparameter quantum metrology is indispensable and thus has received a lot of increasing interest in recent years [29–43], as the number of parameters affecting a physical process is usually more than one. For instance, Humphreys *et al.* [29] treated the phase imaging problem regarded as a multiparameter estimation process, and showed the advantages of the multiparameter simultaneous estimation using the multi-mode NOON state, when comparing with the independent estimation scheme. The advantages remain even if there are photon losses, as studied by Yue *et al.* [30]. Apart from the photon losses, Ho *et al.* [31] estimated three components of an external magnetic field using the entangled Greenberger–Horne–Zeilinger state including the dephasing noise and showed that its sensitivity can beat the SQL. Besides, Yao *et al.* [32] investigated the multiple phase estimation problem for a natural parametrization of arbitrary pure states under the white noise. In order to further develop the quantum enhanced multiparameter simultaneous estimation, Hong *et al.* [33] proposed a method to generate the multi-mode NOON state, and they experimentally demonstrated that the QCRB can be saturated using the multi-mode NOON state. In addition to the NOON state, entangled coherent state is also widely used in the field of quantum metrology. To compare the performance of the entangled coherent state [44, 45] can be better with that of the multi-mode NOON state, Liu *et al.* [34] proposed a theoretical scheme of quantum enhanced multiparameter metrology with generalized entangled coherent state and showed that the entangled coherent state can indeed give better precision than that of the multi-mode NOON state. After that, Zhang *et al.* [43] investigated the quantum multiparameter estimation with generalized balanced multimode NOON-like states, including the entangled squeezed vacuum state (ESVS), the entangled squeezed coherent state, the entangled coherent state, and the NOON state. Comparing with other multimode NOON-like states, they found that the ESVS has the lowest QCRB if the mean photon number is the same. However, how to prepare the multimode ESVS has not yet been studied before. In addition, the maximum average photon number of the squeezing vacuum state achievable currently is still limited (about 15 dB for single mode squeezed vacuum [46] and 10.7 dB for two-mode squeezed vacuum [47]). A natural question is that can we improve the multiparameter estimation further under the same average photon number by performing certain non-Gaussian operation on the ESVS?

In this paper, we propose a scheme to generate the multimode ESVS or the entangled superposition of the photon-catalysis squeezed vacuum state which may find applications in the quantum information and quantum metrology. Due to the fact that the multi-photon catalysis operation [48, 49] can improve the fidelity in quantum teleportation [50, 51], extend the transmission distance in continuous variable quantum key distribution [52, 53], and enhance the sensitivity of phase estimation for a single-phase estimation [19] and undo the noise effect of the channel [54], we also propose a scheme to improve the multiparameter estimation precision by using the MECSVS. Our results clearly show that the multi-photon catalytic operation can further improve the precision of phase estimation compared with the result with ordinary ESVS as the probe state under the same average photon number. Moreover, the usage of multi-photon catalysis in the multiparameter quantum metrology is also more robust against the photon losses which can find applications in the practical scenarios.

The paper is organized as follows. In Section 2, we propose a scheme to generate the MECSVS. In Sections 3 and 4, we evaluate the QCRB of multiparameter estimation with the symmetric MECSVS under ideal and photon-loss cases, respectively. In Section 5, we study the QCRB when the anti-symmetric MECSVS is used. Finally, we summarize the results.

2 The generation of the MECSVS

In this section, we propose a scheme to generate the MECSVS which is the probe quantum state used for the quantum multiparameter estimation. The schematic diagram is shown in Fig. 1 in which three steps are included. In the first step, we perform the n-photon catalysis (orange box) on the input SSVS $|\xi\rangle$. In the n-photon catalysis, an n-photon Fock state $|n\rangle$ in an ancillary mode $\widetilde{a}$ is injected into one port of a beam splitter with a transmissivity T, and then is detected at the corresponding output of mode $\widetilde{a}$. In the meantime, the input squeezed state $|\xi\rangle$ is injected into the other port a of the beam splitter. If n photons are detected at the output port $\widetilde{a}$, the so called n-photon catalysis is performed and the output state of port a is given by $|\xi'\rangle$ which is the single-mode n-photon catalyzed squeezed state. This multi-photon catalyzed process can be regarded as an effective operator [50], i.e.,

$$\begin{aligned}\widehat{O} &\equiv \langle n|\widehat{B}(T)|n\rangle \\ &= \frac{T^{n/2}}{n!}\frac{\partial^n}{\partial\tau^n}\left\{\frac{\exp\left[\mu(\tau)a^\dagger a\right]}{1-\tau}\right\}\Bigg|_{\tau=0},\end{aligned} \tag{1}$$

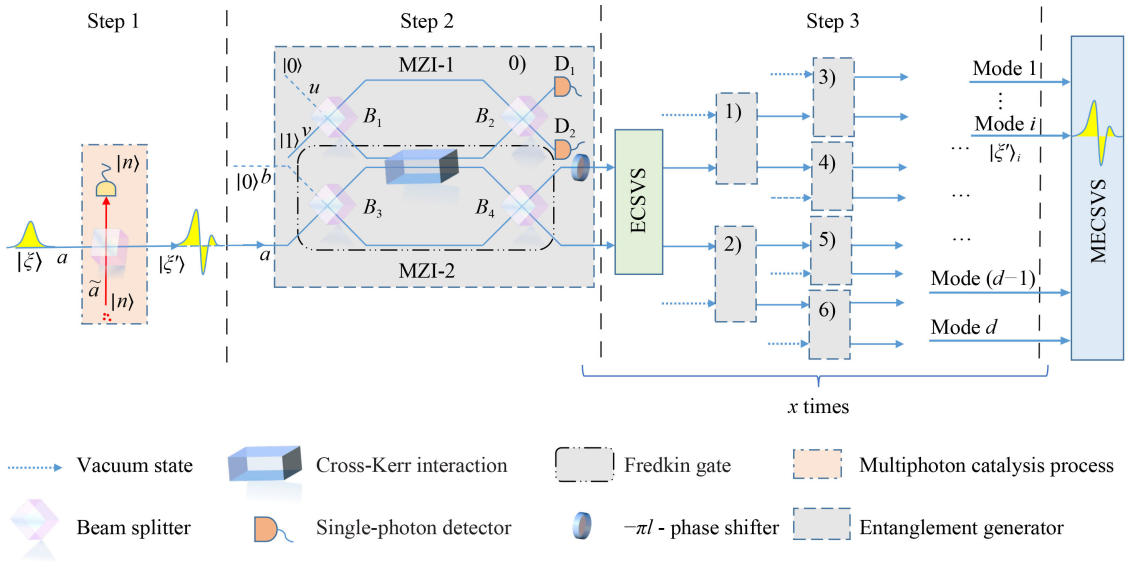

Fig. 1 Generation of the d-mode MECSVS using quantum-optical Fredkin gate. The orange box is the multi-photon catalysis process, in which an n-photon Fock state is inputted into auxiliary mode of beam splitter, conditional measuring n photons at one output. The dashed box is the entanglement generator, which creates two-mode entangled catalysis squeezed vacuum state by using the single-mode multi-photon catalysis squeezed vacuum state and vacuum state. Applying the entanglement generator x times with each input of the following generator aligning with one of the output modes of the previous generator creates a d-mode MECSVS.

where $\widehat{B}(T)=\mathrm{e}^{(\tilde{a}^{\dagger}a-\tilde{a}a^{\dagger})\arccos\sqrt{T}}$ and the parameter

$$\mu(\tau)=\ln\frac{\sqrt{T}-\tau/\sqrt{T}}{1-\tau}. \tag{2}$$

Considering that the input state of a-mode is a Gaussian SSVS $|\xi\rangle=\sqrt{\operatorname{sech}r}\sum_{l=0}^{\infty}\left(-\frac{1}{2}\tanh r\right)^{l}\sqrt{(2l)!}/l!\,|2l\rangle$ as the input state [55], the corresponding single-mode multi-photon catalysis squeezed vacuum state is thus given by

$$\begin{aligned}|\xi'\rangle&=\frac{1}{\sqrt{\mathbb{N}}}\widehat{O}\,|\xi\rangle_a\\&=\frac{1}{\sqrt{\mathbb{N}}}\frac{T^{n/2}}{n!}\frac{\partial^n}{\partial\tau^n}\left[\beta(\tau)\sum_{l=0}^{\infty}c_l(\tau)\,|2l\rangle_a\right]\Big|_{\tau=0},\end{aligned} \tag{3}$$

with $\beta(\tau)=1/(1-\tau)\sqrt{\cosh r}$, $c_l(\tau)=\left[-\frac{1}{2}\mathrm{e}^{2\mu(\tau)}\tanh r\right]^{l}\cdot\sqrt{(2l)!}/l!$ and $\mathbb{N}$ is the success probability given by

$$\mathbb{N}=\frac{T^n}{(n!)^2}\frac{\partial^{2n}}{\partial\tau^n\partial\tau^{*n}}\aleph(\tau,\tau^*)\left[1-\Im(\tau,\tau^*)\right]^{-\frac{1}{2}}\Big|_{\tau=\tau^*=0}, \tag{4}$$

with

$$\begin{aligned}\aleph(\tau,\tau^*)&=\frac{1}{(1-\tau)(1-\tau^*)\cosh r},\\\Im(\tau,\tau^*)&=\mathrm{e}^{2[\mu(\tau^*)+\mu(\tau)]}\tanh^2 r,\end{aligned} \tag{5}$$

where τ^* is the complex conjugate of τ. In particular, from Eq. (3), when $T=1$, the single-mode multi-photon catalysis squeezed vacuum state is reduced to the SSVS, as expected. Although the photon catalysis operation is probabilistic [56], it can be heralded and we choose to perform the quantum metrology only when the MECSVS is successfully generated.

After generating the single-mode multi-photon catalysis squeezed vacuum state as shown in Eq. (3), we next produce a two-mode multi-photon catalysis squeezed vacuum state using step 2 as shown in Fig. 1. For this purpose, we propose to employ that quantum-optical Fredkin gate which consists of two Mach–Zehnder interferometers mediated by a cross-Kerr medium. To be more specific, the single-mode multi-photon catalysis squeezed vacuum states and a vacuum state $|0\rangle$ are respectively injected into a cross-Kerr medium based Mach–Zehnder interferometer (MZI-2) from modes a and b. Simultaneously, a vacuum state $|0\rangle_u$ and a single photon state $|1\rangle_v$ are used as inputs of the MZI-1. We assume that the four beam splitters $\widehat{B}_j$ $(j=1,2,3,4)$ are chosen as 50:50, i.e., $\widehat{B}_1=\mathrm{e}^{\mathrm{i}\pi\left(u^{\dagger}v+uv^{\dagger}\right)/4}$ and $\widehat{B}_3=\mathrm{e}^{\mathrm{i}\pi\left(a^{\dagger}b+ab^{\dagger}\right)/4}$ with $\widehat{B}_4=\widehat{B}_3^{\dagger}$ and $\widehat{B}_2=\widehat{B}_1^{\dagger}$. After passing through the beams splitters B_1 and B_3, the photons in mode a and mode u pass through the corss-Kerr medium at the same time and the effective operator is given by [57, 58]

$$\widehat{U}_k=\exp\left(\mathrm{i}\chi t a^{\dagger}a u^{\dagger}u\right), \tag{6}$$

where χ is the nonlinear Kerr coupling coefficient and t is the interaction time. For our purpose here, we choose $\chi t=\pi$. Unfortunately, the cross-Kerr nonlinearity in the

natural medium is usually very small and χt is usually much less than π. However, enhancement of the cross-Kerr nonlinearity is not impossible. In the past few decades, a number of methods have been proposed to achieve giant Kerr nonlinearity. For example, giant Kerr-nonlinearity such that $\chi > 2\pi \times 10^{10}$ Hz can be achieved in an atomic ensemble by the electromagnetic induced transparency (EIT) and the slow light effect [59–63]. Besides, in Ref. [64], the author showed that by constructing a one-dimensional nonlinear photonic crystal from alternating layers of Kerr medium and linear dielectric medium, the phase of the wave function of the incident photons can be rotated by π phase. In addition, by measurement-induced quantum operations, Costanzo *et al.* [65] demonstrated an experimental implementation of a strong Kerr nonlinearity where a π phase shift is realized. Therefore, π phase shift by the Kerr-type interaction is possible.

It is clearly seen that if the u-mode is vacuum, no phase shift for the b mode. However, if the u-mode has 1 photon, there is a phase shift for the b mode. Due to the phase shift, the b-mode may enter the upper path or lower path after passing through B_4. This is the basic principle for generating the entangled state in this setup. The combination of the operation $\widehat{U}_F = \widehat{B}_4\widehat{U}_k\widehat{B}_3$ is actually the quantum-optical Fredkin gate which is given by

$$\widehat{U}_F = \mathrm{e}^{\mathrm{i}\frac{\pi}{2}u^\dagger u\left(a^\dagger a+b^\dagger b\right)}\mathrm{e}^{\frac{\pi}{2}u^\dagger u\left(ab^\dagger-a^\dagger b\right)}. \tag{7}$$

This quantum gate can effectively entangle the two photon modes.

To be more specific, when $|\xi'\rangle$ and $|0\rangle$ are injected into the MZI-2 ($|0\rangle_u$ and $|1\rangle_v$ are injected into the MZI-1), the unnormalized output state can be expressed as

$$\begin{aligned}&\widehat{B}_2\widehat{B}_4\widehat{U}_k\widehat{B}_3\widehat{B}_1\left|\xi'\right\rangle_a\left|0\right\rangle_b\left|0\right\rangle_u\left|1\right\rangle_v\\ =&\frac{1}{2}[\left(\left|0\right\rangle_a\left|\mathrm{e}^{\mathrm{i}\pi l}\xi'\right\rangle_b+\left|\xi'\right\rangle_a\left|0\right\rangle_b\right)\left|1\right\rangle_u\left|0\right\rangle_v\\ &+\mathrm{i}\left(-\left|0\right\rangle_a\left|\mathrm{e}^{\mathrm{i}\pi l}\xi'\right\rangle_b+\left|\xi'\right\rangle_a\left|0\right\rangle_b\right)\left|0\right\rangle_u\left|1\right\rangle_v].\end{aligned} \tag{8}$$

Here, the state $\left|\mathrm{e}^{\mathrm{i}\pi l}\xi'\right\rangle_b$ describes the state similar to Eq. (3) but the coefficient $c_l(\tau)$ is multiplied by a phase factor $\mathrm{e}^{\mathrm{i}\pi l}$. To remove this additional phase shift, we place a quarter wave plate in the output route of b mode. When $2l$ photons pass through this quarter wave plate, an additional πl phase shift is accumulated which exactly cancels out the previous phase factor. Two single photon detectors D_1 and D_2 are placed in the output routes of u and v modes. According to Eq. (8), the output state depends on the detection results of u and v modes. Finally, the output state is given by

$$\left|\psi\right\rangle_{ab} = \frac{1}{\sqrt{\widetilde{N}_2}}(\pm\left|0\right\rangle_a\left|\xi'\right\rangle_b+\left|\xi'\right\rangle_a\left|0\right\rangle_b), \tag{9}$$

where $\widetilde{N}_2$ is a normalization factor. The symmetric (anti-symmetric) state is obtained when a single photon is detected in D_1 (D_2) and no photon is detected in D_2 (D_1). It is clearly seen that the two-mode ECSVS is generated. Both the symmetric and the antisymmetric ECSVSs can be used for improving the precision of the metrology. In the following, we mainly consider the symmetric case and disscuss the antisymmetric case in Section 5.

After preparing the two-mode ECSVS state, we use it as inputs of two MZIs and repeat the procedures as those in step 2. By repeating these procedures for a number of time, we can in principle generate the MECSVS. If all the detection results of the auxiliar qubits are one photon in the mode u and zero photon in the mode v, the output state is then given by

$$\left|\Psi\right\rangle = \frac{1}{\sqrt{\widetilde{\mathbb{N}}}}\sum_{j=0}^{d}\left|0\right\rangle_0\left|0\right\rangle_1\left|0\right\rangle_2\left|0\right\rangle_3\ldots\left|\xi'\right\rangle_j\ldots\left|0\right\rangle_d, \tag{10}$$

where $\widetilde{\mathbb{N}} = (d+1)\left(1+d\left|\langle 0|\,\xi'\rangle\right|^2\right)$ is the normalized coefficient, which can be calculated as

$$\begin{aligned}\widetilde{\mathbb{N}} =&\frac{T^n}{(n!)^2}\frac{\partial^{2n}}{\partial\tau^n\partial\tau^{*n}}(d+1)\,\aleph\left(\tau,\tau^*\right)\\ &\times\left\{\left[1-\Im\left(\tau,\tau^*\right)\right]^{-1/2}+d\right\}\Big|_{\tau=\tau^*=0}.\end{aligned} \tag{11}$$

We note that $\widetilde{\mathbb{N}} \geq d+1$ because $\left|\langle 0|\,\xi'\rangle\right|^2 \geq 0$. Therefore, the average photon number of the symmetric superposition of the MECSVS $\bar{n} = (d+1)\langle\xi'|a^\dagger a|\xi'\rangle/\widetilde{\mathbb{N}}$ is usually smaller than the average photon number of the single mode catalysis squeezed vacuum state $\langle\xi'|a^\dagger a|\xi'\rangle$. When ξ' is the squeezed vacuum, we can see that the average photon number of the symmetric superposition of ESVS is usually smaller than that of the single-mode SVS, i.e., $\sinh^2 r$. The quantum state shown in Eq. (10) is a symmetric MECSVS which is a highly entangled state. In particular, when $T = 1$, the MECSVS is reduced to the multi-mode ESVS, as expected. In the following, we shall use the MECSVS as the inputs of a multi-arm interferometer in order to effectively improve the precision of multiparameter estimations of multiple optical phases at the same time with and without photon losses.

3 The QCRB of multiparameter estimation without photon losses

In this section, we investigate the QCRB of multiple independent phases estimation simultaneously by a multi-arm interferometer with inputting the MECSVS shown in Eq. (10) under the ideal case. The schematic diagram of d parameters estimation is shown in Fig. 2 where the mode 0 is the reference beam and the modes from 1 to d are the parametric beams. The d estimated parameters are assumed to be mutually independent linear phases and their transformations through the multi-arm interferometer can be represented by a unitary operator [29, 43]

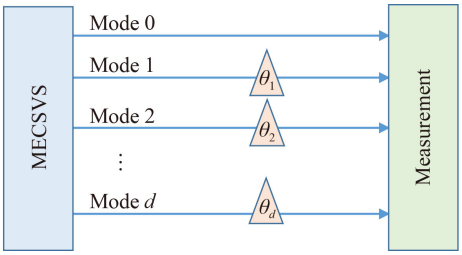

Fig. 2 Schematic of multiparameter estimation with d phase shifts under an ideal case.

$$\widehat{U}_\theta = \exp\left(\mathrm{i}\sum_{j=1}^{d}\theta_j\cdot\widehat{N}_j\right), \tag{12}$$

where θ_j and $\widehat{N}_j = a_j^\dagger a_j$ represent the phase shift and the photon number operator for the jth mode, respectively. Since all the phases are independent to each other, the photon number operators $\widehat{N}_j$ for different j are commutable. When the input MECSVS $|\Psi\rangle$ goes through the interferometer, the output state can be expressed as $|\Psi_{out}\rangle = \widehat{U}_\theta|\Psi\rangle$. According to the definition of QCRB, the estimation precision of $\widehat{\theta}$ is inversely proportional to the quantum Fisher inforamtion (QFI) of the output state $|\Psi_{out}\rangle$, i.e.,

$$\left|\Delta\widehat{\theta}\right|^2 \geq \left|\Delta\widehat{\theta}\right|^2_{QCRB} = \mathrm{Tr}[\boldsymbol{F}_\theta^{-1}], \tag{13}$$

where $|\Delta\widehat{\theta}|^2$ is the total variance as a figure of merit for the multiparameter estimation [34], $\mathrm{Tr}[\cdot]$ represents the trace operation and $\boldsymbol{F}_\theta^{-1}$ is the inverse of the $d\times d$ QFI matrix. Given an arbitrary pure state, it is possible to saturate the QCRB if $\mathrm{Im}\langle\psi|L_jL_k|\psi\rangle = 0$ is satisfied for all j,k and θ, in which $L_{j(k)}$ is the symmetric logarithmic derivative given by $L_{j(k)} = 2\left(|\partial_{j(k)}\Psi_{out}\rangle\langle\Psi_{out}| + |\Psi_{out}\rangle\langle\partial_{j(k)}\Psi_{out}|\right)$ with $|\partial_{j(k)}\Psi_{out}\rangle = \partial_{j(k)}|\Psi_{out}\rangle/\partial_{j(k)}\theta_{j(k)}$ [66, 67]. For our scheme, based on Eqs. (10) and (12), the elements of the QFI matrix are given by

$$f_{jk} = 4(\langle\Psi|\widehat{N}_j\widehat{N}_k|\Psi\rangle - \langle\Psi|\widehat{N}_j|\Psi\rangle\langle\Psi|\widehat{N}_k|\Psi\rangle). \tag{14}$$

As a result, the QFI matrix reads as [68]

$$\boldsymbol{F}_\theta = 4\frac{1}{\widetilde{\mathbb{N}}}\langle\xi'|\widehat{N}^2|\xi'\rangle I - 4\frac{1}{\widetilde{\mathbb{N}}^2}\langle\xi'|\widehat{N}|\xi'\rangle^2\bar{I}, \tag{15}$$

where I represents the identity matrix and $\bar{I}$ denotes the matrix with the elements $\bar{I}_{jk} = 1$ for all j and k. From Eqs. (13) and (15), we can finally obtain the expression of the QCRB for our scheme [34], i.e.,

$$|\Delta\widehat{\theta}|^2_{QCRB} = \frac{d}{4\langle\xi'|\widehat{N}^2|\xi'\rangle}\left(\widetilde{\mathbb{N}} + \frac{1}{\mathbb{k} - d/\widetilde{\mathbb{N}}}\right), \tag{16}$$

where $\mathbb{k} = \langle\xi'|\widehat{N}^2|\xi'\rangle/\langle\xi'|\widehat{N}|\xi'\rangle^2$ with

$$\begin{aligned}\langle\xi'|\widehat{N}^2|\xi'\rangle =& \frac{T^n}{(n!)^2}\frac{\partial^{2n}}{\partial\tau^n\partial\tau^{*n}}\aleph(\tau,\tau^*)\\ &\times\frac{\Im(\tau,\tau^*)\left[\Im(\tau,\tau^*)+2\right]}{\left[1-\Im(\tau,\tau^*)\right]^{5/2}}|_{\tau=\tau^*=0},\\ \langle\xi'|\widehat{N}|\xi'\rangle =& \frac{T^n}{(n!)^2}\frac{\partial^{2n}}{\partial\tau^n\partial\tau^{*n}}\aleph(\tau,\tau^*)\\ &\times\frac{\Im(\tau,\tau^*)}{\left[1-\Im(\tau,\tau^*)\right]^{3/2}}|_{\tau=\tau^*=0}.\end{aligned} \tag{17}$$

Note that $|\Delta\widehat{\theta}|^2_{QCRB}$ is positive definite according to Eq. (16). Especially, when $T=1$, one can obtain $\langle\xi'|\widehat{N}^2|\xi'\rangle = \sinh^4 r + 2\sinh^2 r\cosh^2 r$ and $\langle\xi'|\widehat{N}|\xi'\rangle = \sinh^2 r$, which is consistent with the result of the $d+1$ modes ESVS case, as expected [43]. When $T\neq 1$, the QCRB can be different from that of the ESVS case.

To elaborate the advantages of the MECSVS as inputs of the multi-arm interferometer, we plot the $|\Delta\widehat{\theta}|^2_{QCRB}$ as a function of the mean photon number for several different catalytic photon numbers $n\in\{1,2,3\}$, as shown in Fig. 3 where $d=5$ and $T=0.7,0.8,0.9$. As a comparison, the black solid line corresponds to the result using the multi-mode ESVS case. It is clearly seen that the QCRBs in the case using MECSVS as inputs are

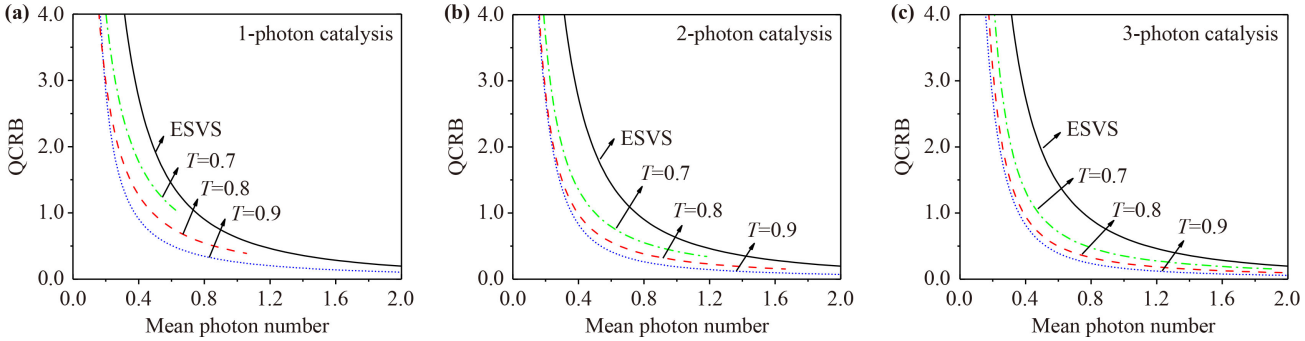

Fig. 3 The QCRB as a function of mean photon number for the ESVS (black) and the MECSVSs with $T=0.9$ (blue), $T=0.8$ (red), and $T=0.7$ (green). **(a)** The case of single-photon catalytic, **(b)** the case of two-photon catalytic, **(c)** the case of three-photon catalytic.

obviously lower than those using the normal ESVS for all three catalytic photon numbers (i.e., $n = 1, 2$ or 3) especially when the average photon number is small. This indicates that by catalyzing the SSVS before inputting into the interferometer we can significantly improve the phase detection precision. The QCRB is the lowest when $T = 0.9$ comparing with $T = 0.7$ and $T = 0.8$ for all three catalytic photon numbers. We also note that the mean photon number of the MECSVS increases with the squeezing parameter r but is saturated when r is large enough (see Fig. 4). The maximum reachable mean photon number increases when T or the catalysis photon number increases. In Fig. 3 we mainly show the improvement of precision in the range of low photon number. This may find applications in the situation where the disturbance to the system needs to be minimized when the phases are measured. Despite that we mainly show the improvement in the low photon number range, the improvement when the photon number is relatively large can also be achieved if the transmissivity T or the number of photon catalysis increase (see Fig. 4) or the antisymmetric state is used for the metrology (see Fig. 8 in Section 5).

4 The QCRB of the multiparameter estimation with photon losses

Under the realistic environment, photon losses and phase diffusions are usually unadvoidable, which can affect the ultimate precision limit of the optical interferometry. Here we focus on studying the QCRB of multiparameter estimation with photon losses, as shown in Fig. 5. To describe the influences of noise environment on the phase probing system S, additional degrees of freedom should be introduced, i.e., the environment denoted as E. Here we assume that the environment is in the vacuum state which is a reasonable assumption for the optical regime. In such circumstance, the initial state of the system and the environment are separable and can be written as $|\Psi\rangle_S |\mathbf{0}\rangle_E$. The evolution of the whole combined system is unitary and can be denoted as $\widehat{U}^{S+E}(\theta)$. Thus, the final state before the measurement can be expressed as [69]

$$|\Psi(\theta)\rangle_{S+E} = \widehat{U}^{S+E}(\theta)\,|\Psi\rangle_S\,|\mathbf{0}\rangle_E = \sum_{\boldsymbol{k}} \widehat{\Pi}_{\boldsymbol{k}}(\theta)\,|\Psi\rangle_S\,|\boldsymbol{k}\rangle_E\,, \tag{18}$$

where $\widehat{U}^{S+E}(\theta) = U_0^{S_0+E_0} U_1^{S_1+E_1}(\theta_1)....U_d^{S_d+E_d}(\theta_d)$ and the environment vacuum state $|\mathbf{0}\rangle_E = |\mathbf{0}\rangle_{E_0}|\mathbf{0}\rangle_{E_1}....|\mathbf{0}\rangle_{E_d}$. In the second identity, $|\boldsymbol{k}\rangle_E = |k_0\rangle_{E_0}|k_1\rangle_{E_1}...|k_d\rangle_{E_d}$ are orthonormal states of the environment, and $\widehat{\Pi}_{\boldsymbol{k}}(\theta) = \widehat{\Pi}_{k_0}(\theta_0) \otimes \widehat{\Pi}_{k_1}(\theta_1)....\otimes\widehat{\Pi}_{k_d}(\theta_d)$ is the tensor product of all Kraus operator $\widehat{\Pi}_{k_j}(\theta_j)$ [70, 71], each of which is defined as

$$\widehat{\Pi}_{k_l}(\theta_l) = {}_{E_l}\langle k|\widehat{U}_l^{S_l+E_l}(\theta_l)\,|0\rangle_{E_l}\,. \tag{19}$$

From Eq. (18), we can then calculate the QFI matrix of the whole system including the noisy environment and the QFI matrix elements is given by

$$F(\theta, \widehat{\Pi}_{\boldsymbol{k}}(\theta))_{lj} = 4(\langle\widehat{\mathfrak{L}}^{(lj)}\rangle - \langle\widehat{\Gamma}^{(l)}\rangle\langle\widehat{\Gamma}^{(j)}\rangle), \tag{20}$$

where $\langle\cdot\rangle$ standing for $\langle\Psi|\cdot|\Psi\rangle$ and

$$\widehat{\Gamma}^{(l)} = \sum_{k_l} \mathrm{i}\frac{\mathrm{d}\widehat{\Pi}_{k_l}^{\dagger}(\theta_l)}{\mathrm{d}\theta_l}\widehat{\Pi}_{k_l}(\theta_l)\,, \tag{21}$$

$$\widehat{\mathfrak{L}}^{(lj)} = \begin{cases} \sum_{k_l} \frac{\mathrm{d}\widehat{\Pi}_{k_l}^{\dagger}(\theta_l)}{\mathrm{d}\theta_l}\frac{\mathrm{d}\widehat{\Pi}_{k_l}(\theta_l)}{\mathrm{d}\theta_l}, l = j, \\ \widehat{\Gamma}^{(l)}\widehat{\Gamma}^{(j)}, l \neq j. \end{cases} \tag{22}$$

As an example of the noise environment, the photon loss can be simulated using an optical beam splitter with a transmissivity η_l ($\eta_l = 1$ corresponds to lossless case, and $\eta_l = 0$ corresponds to complete photon loss). From Eqs. (19), (21) and (22), we can obtain $\widehat{\Gamma}^{(l)} = \mu_l\widehat{N}_l$ and $\widehat{\mathfrak{L}}^{(ll)} = \mu_l\widehat{N}_l^2 + v_l\widehat{N}_l$ when $l = j$ (and $\widehat{\mathfrak{L}}^{(lj)} = \widehat{\Gamma}^{(l)}\widehat{\Gamma}^{(j)}$ when $l \neq j$), with $\mu_l = 1 - (1+\varepsilon_l)(1-\eta_l)$ and $v_l = (1+\varepsilon_l)^2\eta_l(1-\eta_l)$. As shown in Fig. 5, if such photon losses exist in the each mode of the multi-arm interferometer, a series of Kraus operators in each mode is given by [30]

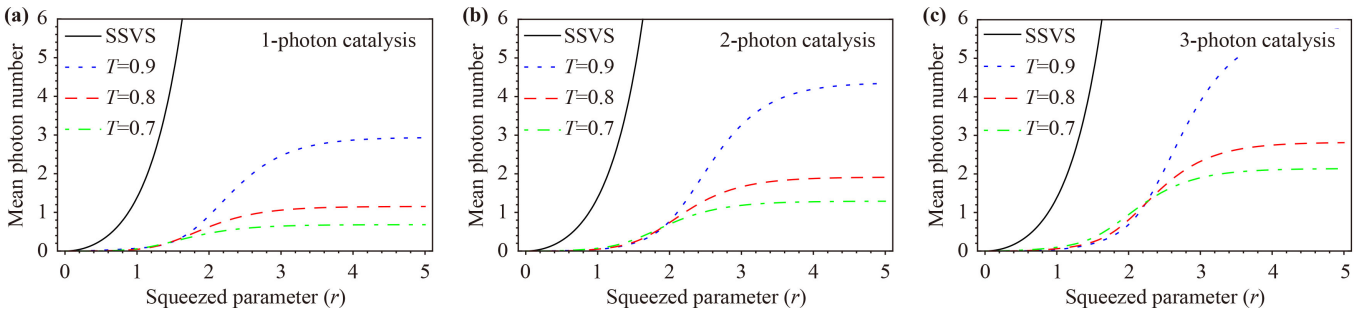

Fig. 4 The mean photon number as a function of mean photon number for the MECSVSs with $T = 0.9$ (blue), $T = 0.8$ (red), and $T = 0.7$ (green). **(a)** the case of single-photon catalytic, **(b)** the case of two-photon catalytic, **(c)** the case of three-photon catalytic. The corresponding mean photon number of the SSMS is also plotted (see black line).

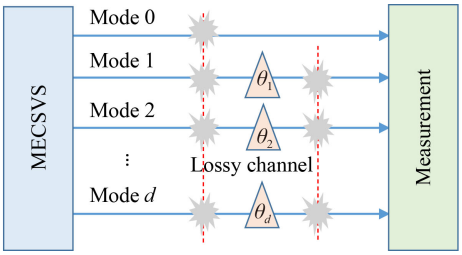

Fig. 5 Schematic of multiparameter estimation with d phase shifts under the photon losses.

$$\widehat{\Pi}_{k_l}(\theta_l)=\sqrt{\frac{(1-\eta_l)^{k_l}}{k_l}}\mathrm{e}^{\mathrm{i}\theta_l\left(\widehat{N}_l-\varepsilon_l k_l\right)}\eta_l^{\frac{\widehat{N}_l}{2}}a_l^{k_l}, \tag{23}$$

where ε_l is an arbitrary real number. ε_l need to be optimized to make the lower bound $F(\theta,\widehat{\Pi}_{\boldsymbol{k}})$ as tight as possible. According to Eqs. (20) and (23), the lower bound for the optimal precision of multiparameter estimation is given by [72, 73]

$$\mathrm{cov}(\theta)\geq\frac{1}{F(\theta,\widehat{\Pi}_{\boldsymbol{k}})}. \tag{24}$$

Based on Eq. (24), let us take the MECSVS as the input of multi-arm interferometer. In this case, all (off-) diagonal elements of $F(\theta,\widehat{\Pi}_{\boldsymbol{k}})$ are the same, denoted as F_d (F_o). For simplicity, here we can make a reasonable assumption that $\eta_l=\eta$ and $\varepsilon_l=\varepsilon$ since all modes are symmetric for the probe state and then we can obtain

$$F_d=4(\mu_l^2\langle\Delta\widehat{N}_l^2\rangle+v_l\langle\widehat{N}_l\rangle), \tag{25}$$

$$F_o=4[\mu_l^2(\langle\widehat{N}_l\widehat{N}_j\rangle-\langle\widehat{N}_l\rangle\langle\widehat{N}_j\rangle)], \tag{26}$$

where $\langle\Delta\widehat{N}_l^2\rangle=\langle\widehat{N}_l^2\rangle-\langle\widehat{N}_l\rangle^2$ and $\langle\widehat{N}_l\widehat{N}_j\rangle=0$, $\langle\widehat{N}_l\rangle\langle\widehat{N}_j\rangle=\langle\widehat{N}_l\rangle^2$ for the MECSVS. Then we can calculate the analytical expression of the QCRB with MECSVS as inputs of the multi-arm interferometer under the photon losses [30]

$$\left|\Delta\widehat{\theta}\right|^2_{QCRB}=\max_{\widehat{\Pi}_{\boldsymbol{k}}}\mathrm{Tr}[F^{-1}(\theta,\widehat{\Pi}_{\boldsymbol{k}})], \tag{27}$$

where

$$\mathrm{Tr}[F^{-1}(\theta,\widehat{\Pi}_{\boldsymbol{k}})]=\frac{d-1}{F_d-F_o}+\frac{1}{F_d+(d-1)F_o}. \tag{28}$$

In Fig. 6(a), we compare the QCRBs of the ideal (solid lines) and the photon-loss (dashed lines) cases with different input states (i.e., the ESVS and the single-photon catalyzed state) where the strength of the photon loss is chosen to be $\eta=0.9$. We can see that with photon loss, the QCRBs increase for both inputs. However, we can see that the QCRB of using the single-photon catalyzed state is still lower than that using the ESVS case which indicates that the single-photon catalyzed state still has better performance than the ESVS case under the photon losses. We also find that when the mean photon number is less than 0.32, the QCRB for the MECSVS with $n=1$ with photon losses can be still lower than that for the multi-mode ESVS without photon losses. In addition, we also consider the QCRB with the input MECSVS for several different catalytic photon numbers $n\in\{1,2,3\}$, as shown in Fig. 6(b) where $\eta=0.9$. It is found that, the QCRBs for all the three catalysis photon numbers are about the same with photon losses and all of them perform better than that with the ESVS input.

We also investigate the QCRB for different strength of the photon loss which are shown in Fig. 7 where we set $T=0.9$. From the three subfigures, we can see that with the decrease of $\eta\in\{1,0.98,0.96,0.94,0.92,0.90\}$, the QCRB for the MECSVS increases, meaning that the

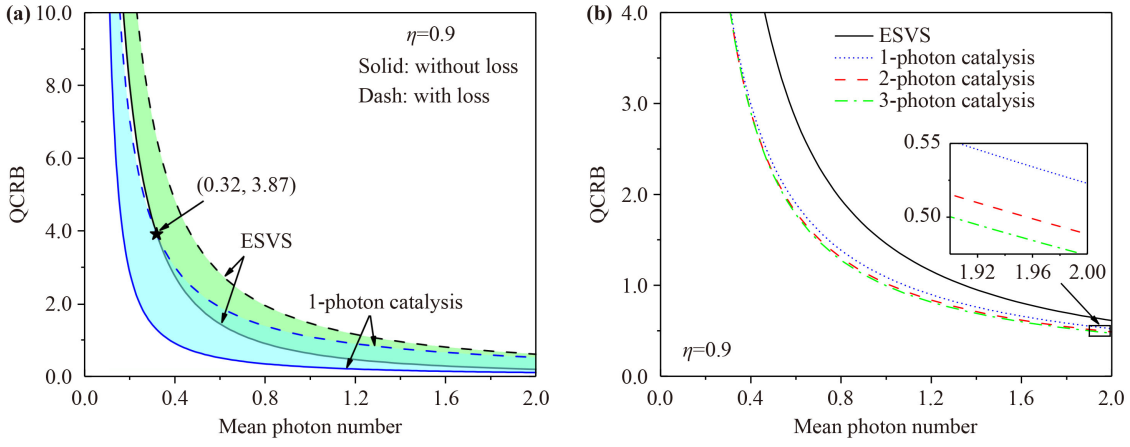

Fig. 6 In the presence of photon losses, the phase uncertainty $|\Delta\widehat{\theta}|^2_{QCRB}$ as a function of the mean photon number. **(a)** Comparison of the ideal case and the loss case for the ESVS and the single-photon catalysis operation. **(b)** Comparison of the phase uncertainty $|\Delta\widehat{\theta}|^2_{QCRB}$ with the number of the photon catalysis $n=1,2$, and 3, and the ESVS (black dashed line) for 10% photon loss ($\eta=0.9$).

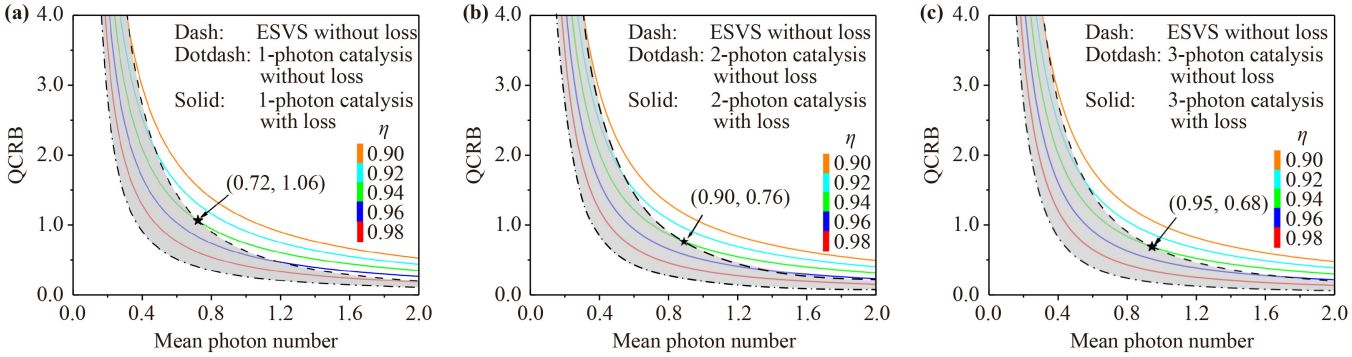

Fig. 7 The QCRB as the function of the mean photon number in the presence of photon losses. The dot line represents the ideal ESVS, the dotdash line represents the single-photon catalytic ESVS, and the colored line represents the QCRB corresponding to different dissipation factors. **(a)** The case of single-photon catalysis, **(b)** the case of two-photon catalysis, **(c)** the case of three-photon catalysis.

precision of multiparameter estimation decreases with the increase of photon-loss intensity. More interestingly, wih the increase of $n = 1, 2, 3$, the usage of the MECSVS with respect to the QCRB canbe superior to that of the multi-mode ESVS at a certain range of the mean photon number. To be more specific, for $\eta = 0.94$ (green line), when the mean photon number is less than $0.72, 0.90$ and 0.95, the QCRB for the MECSVS of $n = 1, 2, 3$ with photon losses can be lower than that for the multi-mode ESVS without photon losses, and such a phenomenon is also true when $\eta = 0.96$ and 0.98. Thus, the results above clearly show that using the MECSVS can improve the phase estimation precision over the ESVS in both the noisy and noisy-free cases.

5 The QCRB of the other multi-mode entangled states

In Section 2, we show that if the measurement results for D_1 and D_2 detectors are zero and one photon, respectively, antisymmetric instead of symmetric superposition of vacuum and ESVS is obtained. In this section, we show that this antisymmetric state can be also used for improving the phase estimation precision. As an example, we assume that all the D_1 and D_2 detectors detect zero and one photon, respectively. In this case, the output state for the 6 modes example (i.e., $d = 5$) can be calculated as

$$\begin{aligned}|\Psi'\rangle =& \frac{1}{\sqrt{\widetilde{\mathbb{N}}'}}(|\xi\rangle_0|0\rangle_1|0\rangle_2|0\rangle_3|0\rangle_4|0\rangle_5 \\ &- |0\rangle_0|\xi\rangle_1|0\rangle_2|0\rangle_3|0\rangle_4|0\rangle_5 \\ &- |0\rangle_0|0\rangle_1|\xi\rangle_2|0\rangle_3|0\rangle_4|0\rangle_5 \\ &+ |0\rangle_0|0\rangle_1|0\rangle_2|\xi\rangle_3|0\rangle_4|0\rangle_5 \\ &- |0\rangle_0|0\rangle_1|0\rangle_2|0\rangle_3|\xi\rangle_4|0\rangle_5 \\ &+ |0\rangle_0|0\rangle_1|0\rangle_2|0\rangle_3|0\rangle_4|\xi\rangle_5), \end{aligned} \tag{29}$$

where $\widetilde{\mathbb{N}}' = (d+1)(1 - |\langle 0|\,\xi'\rangle|^2)$ is the normalization coefficient. Different from the symmetric MECSVS, the normalization factor of the antisymmetric MECSVS $\widetilde{\mathbb{N}}' \leq d+1$ and therefore, the average photon number of the antisymmetric MECSVS can be larger than that of the single-mode CSVS. When ξ' is the squeezed vacuum, we can see that the average photon number of the antisymmetric superposition of ESVS can be larger than that of the single-mode SVS, i.e., $\sinh^2 r$. Based on Eq. (29), we can calculate the QCRB of multiparameter estimations with and without photon losses.

In order to more see whether this entangled state [Eq. (29)] can be also used to improve the precision of multiphase estimation or not, we plot the QCRB as a function of the mean photon number for given $T = 0.9$ and different catalysis photon number $n = 1, 2, 3$ in the ideal case [see Fig. 8(a)] and in the case with photon losses with $\eta = 0.9$ [see Fig. 8(b)]. For comparison, the QCRBs of ESVS as input state with and without photon losses are also shown in the figures. From Fig. 8(a), we can see that, for the entangled state given in Eq. (29), single-photon catalysis and two-photon catalysis have obvious advantages in improving the precision of multiphase estimation. However, when the number of catalytic photons $n \geq 3$, the QCRB of the catalytic entangled states does not surpass that of the ESVS when the mean photon number is large (i.e, larger than 4.13 in this example). From Fig. 8(b), we can see that the QCRB in the case of single-photon catalysis is still lower than that in the ESVS case with photon losses. Hence, using the MECSVS in the antisymmetric case can also improve the phase estimation precision over using the ESVS.

6 Success probability

In this section, we discuss the success probability of our scheme. As known to us, the photon catalysis operation is probabilistic. The success probability depends on the transmissivity of the beam splitter and the number of

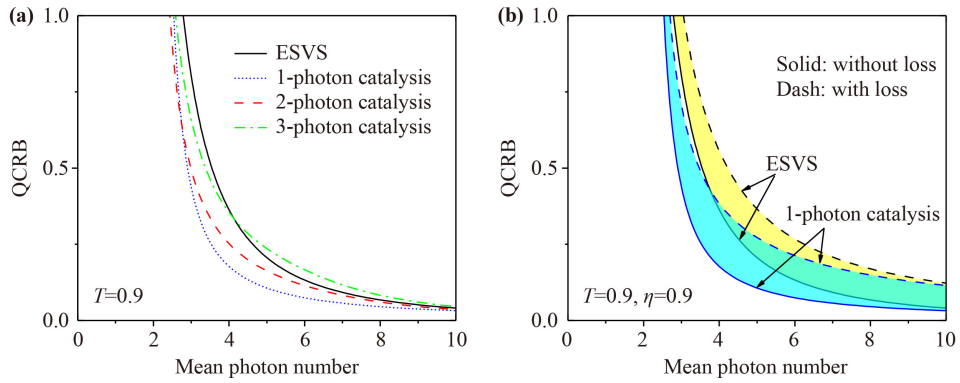

Fig. 8 The QCRB as a function of the mean photon number **(a)** for given $T = 0.9$ and different catalysis photon number $n = 1, 2, 3$ in ideal case and **(b)** for given $T = 0.9$ and $\eta = 0.9$ with photon losses.

photon catalysis which is given by Eq. (4). The higher the transmissivity, the higher the success probability. Fortunately, in our scheme the photon-catalysis is only performed once in the step one shown in Fig. 1 and we find that the improvement of precision is the best when the transmissivity is around 0.9. For this transmissivity, the success probability of the photon catalysis is very high. For example, the success probability is about 70%–90% for the single-photon catalysis, 60%–80% for the two-photon catalysis, and 50%–70% for the three-photon catalysis when the squeezing parameter is in the range between 0 to 1 (Fig. 9).

On the other hand, the quantum-optical Fredkin gate used for the step 2 shown in Fig. 1 is also probabilistic and different measurement results yield different output states. For example, when the photon detector D_1 detects a photon, the output state is the symmetric state $|\psi\rangle_{ab} = (|0\rangle_a|\xi'\rangle_b + |\xi'\rangle_a|0\rangle_b)/\sqrt{N}$, while it is the anti-symmetric state $|\psi\rangle_{ab} = (-|0\rangle_a|\xi'\rangle_b + |\xi'\rangle_a|0\rangle_b)/\sqrt{N'}$ when a single photon is detected in D_2. Despite the different outcomes, both of them can be applied to enhance the sensitivity of the phase measurement. For example, the improvement of phase estimation precision using the symmetric state is shown in Sections 3 and 4 and the improvement of phase estimation precision using the antisymmetric state is discussed in Section 5.

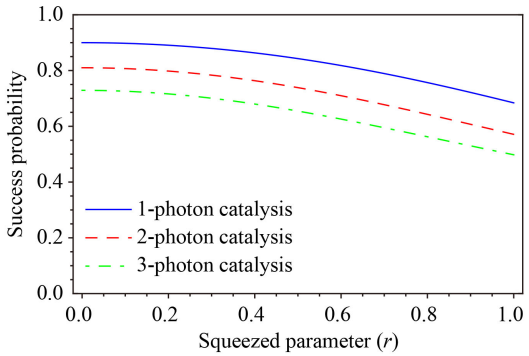

Fig. 9 The success probability of the photon catalysis process as a function of squeezed parameter r for three different number of photon catalysis. The transmissivity $T = 0.9$.

7 Conclusion

In this paper, we first propose a scheme to prepare the ESVS and MECSVS. Then we show that using MECSVS as input of a multi-arm optical interferometer, we can improve the QCRB of the multi-phase measurement over that using the corresponding usual ESVS in both cases with and without photon losses. We also compared the performance of the single-, two-, and three-photon catalysis states. The results shown that in both cases with and without photon losses for the symmetric MECSVS, the three-photon catalysis entangled state have better performance than the other two, which indicates that multi-photon catalysis has more resilient to the environment noises in this case. Additionally, for the antisymmetric MECSVS, it turns out that the single-photon catalyzed entangled state gives the best QCRB, which implies that the MECSVS with antisymmetric case can be also used to improve the phase estimation precision. Our results can find applications in the quantum metrology for multiparameter estimation.

Acknowledgements This work was supported by the National Key R&D Program of China (Grant No. 2021YFA1400800), the Key-Area Research and Development Program of Guangdong Province (Grant No. 2018B030329001), the Natural Science Foundation of Guangdong (Grant No. 2021A1515010039), the National Natural Science Foundation of China (No. 11964013), and the Major Discipline Academic and Technical Leaders Training Program of Jiangxi Province (No. 20204BCJL22053).

Appendix A: Derivation of the two-mode ECSVS [Eq. (9)]

Assume that the initial input state is the single-mode multi-photon catalysis squeezed vacuum state $|\xi'\rangle_a$ [see

Eq. (3)] in the a mode and the vacuum state $|0\rangle_b$ in the b mode. The output state of the step 2 shown in Fig. 1 is given by

$$\begin{aligned}|\psi\rangle &= \widehat{B}_2\widehat{B}_4\widehat{U}_k\widehat{B}_3\widehat{B}_1|\xi'\rangle_a|0\rangle_b|0\rangle_u|1\rangle_v \\ &= \frac{1}{\sqrt{2}}\widehat{B}_2\widehat{U}_F|\xi'\rangle_a|0\rangle_b(|1\rangle_u|0\rangle_v+\mathrm{i}|0\rangle_u|1\rangle_v) \\ &= \frac{1}{\sqrt{2\mathbb{N}}}\widehat{B}_2\frac{T^{n/2}}{n!}\frac{\partial^n}{\partial\tau^n}\beta(\tau)\sum_{l=0}^{\infty}c_l(\tau) \\ &\quad\cdot\mathrm{e}^{\mathrm{i}\chi u^\dagger uJ_0}\mathrm{e}^{\mathrm{i}\chi u^\dagger uJ_2}|2l\rangle_a|0\rangle_b(|1\rangle_u|0\rangle_v+\mathrm{i}|0\rangle_u|1\rangle_v)\Big|_{\tau=0}.\end{aligned} \tag{A1}$$

Since $|n\rangle = a^{\dagger n}/\sqrt{n!}|0\rangle$, Eq. (A1) can be rewritten

$$\begin{aligned}|\psi\rangle =&\frac{1}{\sqrt{2\mathbb{N}}}\widehat{B}_2\frac{T^{n/2}}{n!}\frac{\partial^n}{\partial\tau^n}\beta(\tau)\sum_{l=0}^{\infty}\frac{c_l(\tau)}{\sqrt{(2l)!}}\mathrm{e}^{\mathrm{i}\chi u^\dagger uJ_0} \\ &\cdot\mathrm{e}^{\mathrm{i}\chi u^\dagger uJ_2}a^{\dagger 2l}|0\rangle_a|0\rangle_b(|1\rangle_u|0\rangle_v+\mathrm{i}|0\rangle_u|1\rangle_v)|_{\tau=0}.\end{aligned} \tag{A2}$$

By using the formulas $\mathrm{e}^{\mathrm{i}\chi u^\dagger uJ_i}|1\rangle_u = \mathrm{e}^{\mathrm{i}\chi J_i}|1\rangle_u$, $\mathrm{e}^{\mathrm{i}\chi u^\dagger uJ_i}|0\rangle_u = |0\rangle_u$ with $i=0,2$, $\mathrm{e}^{\mathrm{i}\lambda J_2}a^\dagger\mathrm{e}^{-\mathrm{i}\lambda J_2} = a^\dagger\cos\frac{\lambda}{2} - b^\dagger\sin\frac{\lambda}{2}$ and $\mathrm{e}^{\mathrm{i}\chi u^\dagger uJ_2}|0\rangle_a|0\rangle_b = |0\rangle_a|0\rangle_b$, we can obtain

$$\begin{aligned}|\psi\rangle =&\frac{1}{\sqrt{2\mathbb{N}}}\widehat{B}_2\frac{T^{n/2}}{n!}\frac{\partial^n}{\partial\tau^n}\beta(\tau)\sum_{l=0}^{\infty}\frac{c_l(\tau)}{\sqrt{(2l)!}} \\ &\cdot\mathrm{e}^{\mathrm{i}\chi u^\dagger uJ_0}\left(a^\dagger\cos\frac{\chi}{2}-b^\dagger\sin\frac{\chi}{2}\right)^{2l} \\ &\cdot|0\rangle_a|0\rangle_b(|1\rangle_u|0\rangle_v+\mathrm{i}|0\rangle_u|1\rangle_v)\Big|_{\tau=0} \\ &+\frac{\mathrm{i}}{\sqrt{2\mathbb{N}}}\widehat{B}_2\frac{T^{n/2}}{n!}\frac{\partial^n}{\partial\tau^n}\beta(\tau)\sum_{l=0}^{\infty}\frac{c_l(\tau)}{\sqrt{(2l)!}}a^{\dagger 2l} \\ &\cdot|0\rangle_a|0\rangle_b|0\rangle_u|1\rangle_v\Big|_{\tau=0}.\end{aligned} \tag{A3}$$

Taking $\chi=\pi$ yields

$$\begin{aligned}|\psi\rangle =&\frac{1}{\sqrt{2\mathbb{N}}}\widehat{B}_2\frac{T^{n/2}}{n!}\frac{\partial^n}{\partial\tau^n}\beta(\tau)\times\sum_{l=0}^{\infty}\frac{c_l(\tau)}{\sqrt{(2l)!}}\mathrm{e}^{\mathrm{i}\chi u^\dagger uJ_0} \\ &\cdot\left(-b^\dagger\right)^{2l}|0\rangle_a|0\rangle_b(|1\rangle_u|0\rangle_v+\mathrm{i}|0\rangle_u|1\rangle_v)\Big|_{\tau=0} \\ &+\frac{\mathrm{i}}{\sqrt{2\mathbb{N}}}\widehat{B}_2\frac{T^{n/2}}{n!}\frac{\partial^n}{\partial\tau^n}\beta(\tau)\sum_{l=0}^{\infty}\frac{c_l(\tau)}{\sqrt{(2l)!}}a^{\dagger 2l} \\ &\cdot|0\rangle_a|0\rangle_b|0\rangle_u|1\rangle_v\Big|_{\tau=0}.\end{aligned} \tag{A4}$$

Finally, substituting $J_0 = \frac{1}{2}(a^\dagger a + b^\dagger b)$ into Eq. (A4) and using $\mathrm{e}^{\lambda b^\dagger b}b^\dagger\mathrm{e}^{-\lambda b^\dagger b} = b^\dagger e^{\lambda}$, we can get

$$\begin{aligned}|\psi\rangle =&\frac{1}{\sqrt{2\mathbb{N}}}\widehat{B}_2\frac{T^{n/2}}{n!}\frac{\partial^n}{\partial\tau^n}\beta(\tau) \\ &\cdot\sum_{l=0}^{\infty}\frac{c_l(\tau)}{\sqrt{(2l)!}}\mathrm{e}^{\mathrm{i}\pi l}b^{\dagger 2l}|0\rangle_a|0\rangle_b|1\rangle_u|0\rangle_v\Big|_{\tau=0} \\ &+\frac{\mathrm{i}}{\sqrt{2\mathbb{N}}}\widehat{B}_2\frac{T^{n/2}}{n!}\frac{\partial^n}{\partial\tau^n}\beta(\tau) \\ &\cdot\sum_{l=0}^{\infty}\frac{c_l(\tau)}{\sqrt{(2l)!}}a^{\dagger 2l}|0\rangle_a|0\rangle_b|0\rangle_u|1\rangle_v\Big|_{\tau=0} \\ =&\frac{1}{\sqrt{2\mathbb{N}}}\widehat{B}_2\frac{T^{n/2}}{n!}\frac{\partial^n}{\partial\tau^n}\beta(\tau) \\ &\cdot\sum_{l=0}^{\infty}c_l(\tau)\,\mathrm{e}^{\mathrm{i}\pi l}|0\rangle_a|2l\rangle_b|1\rangle_u|0\rangle_v\Big|_{\tau=0} \\ &+\frac{\mathrm{i}}{\sqrt{2\mathbb{N}}}\widehat{B}_2\frac{T^{n/2}}{n!}\frac{\partial^n}{\partial\tau^n}\beta(\tau) \\ &\cdot\sum_{l=0}^{\infty}c_l(\tau)|2l\rangle_a|0\rangle_b|0\rangle_u|1\rangle_v\Big|_{\tau=0}.\end{aligned} \tag{A5}$$

In the path of mode b, we place a quarter waveplate to compensate the πl phase shift and the output state is

$$|\psi\rangle = \frac{1}{\sqrt{2}}\widehat{B}_2(|0\rangle_a|\xi'\rangle_b|1\rangle_u|0\rangle_v+\mathrm{i}|\xi'\rangle_a|0\rangle_b|0\rangle_u|1\rangle_v). \tag{A6}$$

Then, after the transformations of the second beam splitter B2 of MZI-1, Eq. (6) becomes

$$\begin{aligned}|\psi\rangle =&\frac{1}{2}[(|0\rangle_a|\xi'\rangle_b+|\xi'\rangle_a|0\rangle_b)|1\rangle_u|0\rangle_v \\ &+\mathrm{i}(-|0\rangle_a|\xi'\rangle_b+|\xi'\rangle_a|0\rangle_b)|0\rangle_u|1\rangle_v].\end{aligned} \tag{A7}$$

From Eq. (A7), we can see that if a single photon is detected in the u mode or in the v mode, we can obtain

$$|\psi\rangle_{out} = \frac{1}{\sqrt{\widetilde{N}_2}}(\pm|0\rangle_a|\xi'\rangle_b+|\xi'\rangle_a|0\rangle_b) \tag{A8}$$

which is the two-mode ECSVS [Eq. (9)].

References

1. C. W. Helstrom, Quantum Detection and Estimation Theory, Academic Press, New York, 1976
2. S. L. Braunstein and C. M. Caves, Statistical distance and the geometry of quantum states, *Phys. Rev. Lett.* 72(22), 3439 (1994)
3. J. Joo, W. J. Munro, and T. P. Spiller, Quantum metrology with entangled coherent states, *Phys. Rev. Lett.* 107(8), 083601 (2011)
4. J. Liu, X. X. Jing, and X. G. Wang, Phase-matching

condition for enhancement of phase sensitivity in quantum metrology, *Phys. Rev. A* 88(4), 042316 (2013)
5. L. J. Fiderer, J. M. E. Fraïsse, and D. Braun, Maximal quantum Fisher information for mixed states, *Phys. Rev. Lett.* 123(25), 250502 (2019)
6. W. Zhong, L. Zhou, and Y. B. Sheng, Double-port measurements for robust quantum optical metrology, *Phys. Rev. A* 103(4), 042611 (2021)
7. J. D. Zhang, C. L. You, C. Li, and S. Wang, Phase sensitivity approaching the quantum Cramer–Rao bound in a modified *SU*(1, 1) interferometer, *Phys. Rev. A* 103(3), 032617 (2021)
8. M. Eaton, R. Nehra, A. Win, and O. Pfister, Heisenberg limited quantum interferometry with multiphotonsubtracted twin beams, *Phys. Rev. A* 103(1), 013726 (2021)
9. R. Okamoto and T. Tahara, Precision limit for simultaneous phase and transmittance estimation with phase shifting interferometry, *Phys. Rev. A* 104(3), 033521 (2021)
10. S. Y. Lee, Y. S. Ihn, and Z. Kim, Optimal entangled coherent states in lossy quantum-enhanced metrology, *Phys. Rev. A* 101(1), 012332 (2020)
11. P. M. Anisimov, G. M. Raterman, A. Chiruvelli, W. N. Plick, S. D. Huver, H. Lee, and J. P. Dowling, Quantum metrology with two-mode squeezed vacuum: Parity detection beats the Heisenberg limit, *Phys. Rev. Lett.* 104(10), 103602 (2010)
12. L. Pezzé and A. Smerzi, Mach–Zehnder interferometry at the Heisenberg limit with coherent and squeezed-vacuum light, *Phys. Rev. Lett.* 100(7), 073601 (2008)
13. C. Oh, S. Y. Lee, H. Nha, and H. Jeong, Practical resources and measurements for lossy optical quantum metrology, *Phys. Rev. A* 96(6), 062304 (2017)
14. S. Slussarenko, M. M. Weston, H. M. Chrzanowski, L. K. Shalm, V. B. Verma, S. W. Nam, and G. J. Pryde, Unconditional violation of the shot-noise limit in photonic quantum metrology, *Nat. Photonics* 11(11), 700 (2017)
15. L. L. Guo, Y. F. Yu, and Z. M. Zhang, Improving the phase sensitivity of an *SU*(1, 1) interferometer with photon-added squeezed vacuum light, *Opt. Express* 26(22), 29099 (2018)
16. R. Birrittella and C. C. Gerry, Quantum optical interferometry via the mixing of coherent and photon-subtracted squeezed vacuum states of light, *J. Opt. Soc. Am. B* 31(3), 586 (2014)
17. S. Wang, X. X. Xu, Y. J. Xu, and L. J. Zhang, Quantum interferometry via a coherent state mixed with a photonadded squeezed vacuum state, *Opt. Commun.* 444, 102 (2019)
18. D. Braun, P. Jian, O. Pinel, and N. Treps, Precision measurements with photon-subtracted or photon-added Gaussian states, *Phys. Rev. A* 90(1), 013821 (2014)
19. H. Zhang, W. Ye, C. P. Wei, Y. Xia, S. K. Chang, Z. Y. Liao, and L. Y. Hu, Improved phase sensitivity in a quantum optical interferometer based on multi-photon catalytic two-mode squeezed vacuum states, *Phys. Rev. A* 103(1), 013705 (2021)
20. Y. Ouyang, S. Wang, and L. J. Zhang, Quantum optical interferometry via the photon added two-mode squeezed vacuum states, *J. Opt. Soc. Am. B* 33(7), 1373 (2016)
21. M. A. Taylor and W. P. Bowen, Quantum metrology and its application in biology, *Phys. Rep.* 615, 1 (2016)
22. N. P. Mauranyapin, L. S. Madsen, M. A. Taylor, M. Waleed, and W. P. Bowen, Evanescent single-molecule biosensing with quantum-limited precision, *Nat. Photonics* 11(8), 477 (2017)
23. M. A. Taylor, J. Janousek, V. Daria, J. Knittel, B. Hage, H. A. Bachor, and W. P. Bowen, Biological measurement beyond the quantum limit, *Nat. Photonics* 7(3), 229 (2013)
24. M. Tsang, R. Nair, and X. M. Lu, Quantum theory of superresolution for two incoherent optical point sources, *Phys. Rev. X* 6(3), 031033 (2016)
25. L. J. Fiderer, T. Tufarelli, S. Piano, and G. Adesso, General expressions for the quantum Fisher information matrix with applications to discrete quantum imaging, *PRX Quantum* 2(2), 020308 (2021)
26. C. Lupo, Z. X. Huang, and P. Kok, Quantum limits to incoherent imaging are achieved by linear interferometry, *Phys. Rev. Lett.* 124(8), 080503 (2020)
27. G. Brida, M. Genovese, and I. Ruo Berchera, Experimental realization of sub-shot-noise quantum imaging, *Nat. Photonics* 4(4), 227 (2010)
28. L. Pezzé, Entanglement-enhanced sensor networks, *Nat. Photonics* 15(2), 74 (2021)
29. P. C. Humphreys, M. Barbieri, A. Datta, and I. A. Walmsley, Quantum enhanced multiple phase estimation, *Phys. Rev. Lett.* 111(7), 070403 (2013)
30. J. D. Yue, Y. R. Zhang, and H. Fan, Quantum-enhanced metrology for multiple phase estimation with noise, *Sci. Rep.* 4(1), 5933 (2014)
31. L. B. Ho, H. Hakoshima, Y. Matsuzaki, M. Matsuzaki, and Y. Kondo, Multiparameter quantum estimation under dephasing noise, *Phys. Rev. A* 102(2), 022602 (2020)
32. Y. Yao, L. Ge, X. Xiao, X. G. Wang, and C. P. Sun, Multiple phase estimation for arbitrary pure states under white noise, *Phys. Rev. A* 90(6), 062113 (2014)
33. S. L. Hong, J. Rehman, Y. S. Kim, Y. W. Cho, S. W. Lee, H. Jung, S. Moon, S. W. Han, and H. T. Lim, Quantum enhanced multiple-phase estimation with multi-mode NOON states, *Nat. Commun.* 12(1), 5211 (2021)
34. J. Liu, X. M. Lu, Z. Sun, and X. G. Wang, Quantum multiparameter metrology with generalized entangled coherent state, *J. Phys. A* 49(11), 115302 (2016)
35. Z. B. Hou, R. J. Wang, J. F. Tang, H. D. Yuan, G. Y. Xiang, C. F. Li, and G. C. Guo, Control-enhanced sequential scheme for general quantum parameter estimation at the Heisenberg limit, *Phys. Rev. Lett.* 123(4), 040501 (2019)
36. H. Kwon, Y. Lim, L. Jiang, H. Jeong, and C. Oh, Quantum metrological power of continuous-variable quantum networks, *Phys. Rev. Lett.* 128(18), 180503 (2022)
37. S. S. Pang and A. N. Jordan, Optimal adaptive control for quantum metrology with time-dependent Hamiltonians, *Nat. Commun.* 8(1), 14695 (2017)
38. J. Yang, S. S. Pang, Y. Y. Zhou, and A. N. Jordan, Optimal measurements for quantum multiparameter estimation with general states, *Phys. Rev. A* 100(3), 032104 (2019)
39. R. Nichols, P. Liuzzo-Scorpo, P. A. Knott, and G. Adesso, Multiparameter Gaussian quantum metrology,

Phys. Rev. A 98(1), 012114 (2018)
40. L. Pezzé, M. A. Ciampini, N. Spagnolo, P. C. Humphreys, A. Datta, I. A. Walmsley, M. Barbieri, F. Sciarrino, and A. Smerzi, Optimal measurements for simultaneous quantum estimation of multiple phases, *Phys. Rev. Lett.* 119(13), 130504 (2017)
41. W. Ge, K. Jacobs, Z. Eldredge, A. V. Gorshkov, and M. Foss-Feig, Distributed quantum metrology with linear networks and separable inputs, *Phys. Rev. Lett.* 121(4), 043604 (2018)
42. Z. B. Hou, J. F. Tang, H. Z. Chen, H. D. Yuan, G. Y. Xiang, C. F. Li, and G. C. Guo, Zero-trade-off multiparameter quantum estimation via simultaneously saturating multiple Heisenberg uncertainty relations, *Sci. Adv.* 7(1), eabd2986 (2021)
43. L. Zhang and K. W. C. Chan, Quantum multiparameter estimation with generalized balanced multimode NOON like states, *Phys. Rev. A* 95(3), 032321 (2017)
44. X. X. Jing, J. Liu, W. Zhong, and X. G. Wang, Quantum Fisher information of entangled coherent states in a lossy Mach–Zehnder interferometer, *Commum. Theor. Phys.* 61(1), 115 (2014)
45. J. Joo, K. Park, H. Jeong, W. J. Munro, K. Nemoto, and T. P. Spiller, Quantum metrology for nonlinear phase shifts with entangled coherent states, *Phys. Rev. A* 86(4), 043828 (2012)
46. H. Vahlbruch, M. Mehmet, K. Danzmann, and R. Schnabel, Detection of 15 dB squeezed states of light and their application for the absolute calibration of photoelectric quantum efficiency, *Phys. Rev. Lett.* 117(11), 110801 (2016)
47. Y. J. Wang, W. H. Zhang, R. X. Li, L. Tian, and Y. H. Zheng, Generation of –10.7 dB unbiased entangled states of light, *Appl. Phys. Lett.* 118(13), 134001 (2021)
48. T. J. Bartley, G. Donati, J. B. Spring, X. M. Jin, M. Barbieri, A. Datta, B. J. Smith, and I. A. Walmsley, Multi-photon state engineering by heralded interference between single photons and coherent states, *Phys. Rev. A* 86(4), 043820 (2012)
49. A. I. Lvovsky and J. Mlynek, Quantum-optical catalysis: Generating nonclassical states of light by means of linear optics, *Phys. Rev. Lett.* 88(25), 250401 (2002)
50. L. Y. Hu, Z. Y. Liao, and M. S. Zubairy, Continuous-variable entanglement via multi-photon catalysis, *Phys. Rev. A* 95(1), 012310 (2017)
51. X. X. Xu, Enhancing quantum entanglement and quantum teleportation for two-mode squeezed vacuum state by local quantum-optical catalysis, *Phys. Rev. A* 92(1), 012318 (2015)
52. Y. Guo, W. Ye, H. Zhong, and Q. Liao, Continuousvariable quantum key distribution with non-Gaussian quantum catalysis, *Phys. Rev. A* 99(3), 032327 (2019)
53. W. Ye, H. Zhong, Q. Liao, D. Huang, L. Y. Hu, and Y. Guo, Improvement of self-referenced continuous-variable quantum key distribution with quantum photon catalysis, *Opt. Express* 27(12), 17186 (2019)
54. A. E. Ulanov, I. A. Fedorov, A. A. Pushkina, Y. V. Kurochkin, T. C. Ralph, and A. I. Lvovsky, Undoing the effect of loss on quantum entanglement, *Nat. Photonics* 9, 764 (2015)
55. F. Jia, W. Ye, Q. Wang, L. Y. Hu, and H. Y. Fan, Comparison of nonclassical properties resulting from non-Gaussian operations, *Laser Phys. Lett.* 16(1), 015201 (2019)
56. C. Kumar, Rishabh, and S. Arora, Realistic non-Gaussian-operation scheme in parity-detection-based Mach–Zehnder quantum interferometry, *Phys. Rev. A* 105(5), 052437 (2022)
57. C. C. Gerry and R. A. Campos, Generation of maximally entangled photonic states with a quantum-optical Fredkin gate, *Phys. Rev. A* 64(6), 063814 (2001)
58. N. Imoto, H. A. Haus, and Y. Yamamoto, Quantum nondemolition measurement of the photon number via the optical Kerr effect, *Phys. Rev. A* 32(4), 2287 (1985)
59. H. Schmidt and A. Imamoglu, Giant Kerr nonlinearities obtained by electromagnetically induced transparency, *Opt. Lett.* 21(23), 1936 (1996)
60. D. Vitali, M. Fortunato, and P. Tombesi, Complete quantum teleportation with a Kerr nonlinearity, *Phys. Rev. Lett.* 85(2), 445 (2000)
61. A. B. Matsko, I. Novikova, G. R. Welch, and M. S. Zubairy, Enhancement of Kerr nonlinearity by multiphoton coherence, *Opt. Lett.* 28(2), 96 (2003)
62. H. Kang and Y. F. Zhu, Observation of large Kerr nonlinearity at low light intensities, *Phys. Rev. Lett.* 91(9), 093601 (2003)
63. S. Rebić, J. Twamley, and G. J. Milburn, Giant Kerr nonlinearities in circuit quantum electrodynamics, *Phys. Rev. Lett.* 103(15), 150503 (2009)
64. H. Azuma, Quantum computation with Kerr-nonlinear photonic crystals, *J. Phys. D* 41(2), 025102 (2008)
65. L. S. Costanzo, A. S. Coelho, N. Biagi, J. Fiurášek, M. Bellini, and A. Zavatta, Measurement-induced strong Kerr nonlinearity for weak quantum states of light, *Phys. Rev. Lett.* 119(1), 013601 (2017)
66. A. Fujiwara, Estimation of $SU(2)$ operation and dense coding: An information geometric approach, *Phys. Rev. A* 65(1), 012316 (2001)
67. K. Matsumoto, A new approach to the Cramer–Rao type bound of the pure-state model, *J. Phys. Math. Gen.* 35(13), 3111 (2002)
68. M. G. A. Paris, Quantum Estimation for quantum technology, *Int. J. Quant. Inf.* 7(supp01), 125 (2009)
69. B. M. Escher, R. L. de Matos Filho, and L. Davidovich, General framework for estimating the ultimate precision limit in noisy quantum-enhanced metrology, *Nat. Phys.* 7(5), 406 (2011)
70. M. Sarovar and G. J. Milburn, Optimal estimation of one parameter quantum channels, *J. Phys. Math. Gen.* 39(26), 8487 (2006)
71. H. Zhang, W. Ye, C. P. Wei, C. J. Liu, Z. Y. Liao, and L. Y. Hu, Improving phase estimation using number conserving operations, *Phys. Rev. A* 103(5), 052602 (2021)
72. J. Liu, H. D. Yuan, X. M. Lu, and X. G. Wang, Quantum Fisher information matrix and multiparameter estimation, *J. Phys. A Math. Theor.* 53(2), 023001 (2020)
73. T. Baumgratz and A. Datta, Quantum enhanced estimation of a multidimensional field, *Phys. Rev. Lett.* 116(3), 030801 (2016)